Adiabatic Shear Localization in Titanium and Ti-6 Pct Al-4 Pct V Alloy

H. ANDREW GREBE, HAN-RYONG PAK, and MARC A. MEYERS

Ballistic impact experiments were conducted on 12.5 mm thick commercial purity titanium and Ti-6 pct Al-4 pct V alloy plates using steel "stepped" projectiles with 10.5 mm diameter. The impact velocities varied between 578 m per second and 846 m per second, and a flash X-ray technique was used to determine projectile velocity and to assure the normality of impact. The microstructural damage mechanisms associated with impact (shear band formation, shock wave propagation, and dynamic fracture) were analyzed by optical, and scanning and transmission electron microscopy. Elliptical and spherical cavities were observed along the bands. Microindentation hardness differences between the bands and adjacent regions were slight for the targets; for the projectiles, the hardness in the band was significantly lower than that of surrounding regions. Observation of the fractured regions along the bands showed unique features indicating possible melting. Transmission-electron microscopy of a shear band in titanium revealed microcrystalline features (~0.3 μm diameter) with poorly defined grain boundaries.

I. INTRODUCTION

AN "adiabatic shear band" has been defined[1] as a strain localization phenomenon generally attributed to a plastic instability arising from thermal softening during adiabatic or quasi-adiabatic deformation. Adiabatic shear bands may occur in such diverse areas as ballistic impact, explosive fragmentation machining, grinding, high-velocity fabrication, wear, and low-temperature deformation. While they have been observed since the beginning of this century (as reported by Reference 2) and described by Trent[3] in 1941, their discovery is usually attributed to Zener and Hollomon,[4] in 1944. Reviews on the subject have been published by Bedford *et al.*,[2] Rogers,[3] and Olson *et al.*[1] The investigations on adiabatic shear bands have in general been conducted along two directions: mechanical and microstructural. The mechanical analyses are attempts at determining criteria for the formation of these instabilities of plastic flow. Following the qualitative description of Zener and Hollomon,[4] Recht,[5] Culver,[6] Erlich *et al.*,[7] Clifton,[8] and Bai[9] developed theoretical analyses for shear-band formation. Basinski,[10] Chin *et al.*,[11] and Argon[12] have investigated the phenomenon at low strain rates. Staker[13] recently compared theoretical predictions with actual observations for AISI 4340 steel in a number of heat treatment conditions. The microstructural characterization has been reported in numerous papers for a number of alloy systems. Rogers[3] has classified the bands into "deformed" and "transformed" types: for the latter type, the intense heat evolution, plastic deformation, and rapid cooling after deformation produce phase transformations. Critical to the understanding of adiabatic shear bands is the identification of the microstructure inside the bands. These bands being typically only a few micrometers thick have made this a difficult task, and transmission electron microscopy has been the principal tool. The first study, by Stock and Thompson,[14] dates from 1969. They identified shear instabilities in 2014 aluminum alloy in the aged (T6 condition) and overaged conditions. They found small regions resembling grains (0.3 to 0.6 μm) with misorientations of 5 to 15 deg between them. These grains resembled very much the ones found by Thomas and Willens[15] after rapidly quenching molten aluminum. Craig and Stock[16] investigated 70-30 brass subjected to impact and observed rings in the diffraction pattern; they identified elongated grains (0.1 *vs* 0.2 μm) in the shear bands. This work was followed by two independent observations on armor plate steel.[17,18] Glenn and Leslie[17] investigated a steel (1.0 pct Ni; 0.6 pct C; 0.5 pct Mo; 0.5 pct Cr) in the quenched and tempered condition, impacted by a 0.50 cal projectile. Selected area diffraction patterns covering an area as small as 1.3 μm showed rings, indicating that the individual grain size was much smaller than that (~0.1 μm). Wingrove[18] studied the formation of shearing of a 1 pct carbon, 1 pct chromium steel in the quenched and tempered condition. Although he observed a high density of dislocations and some cell boundaries, with rings in the diffraction patterns, it is not certain whether he was able to identify the structure of the band or a region adjacent to it. Me-Bar and Shechtman[19] recently investigated a titanium-6 pct Al-4 pct V alloy after various heat treatments. They observed ring-like diffraction patterns and described the substructure inside the band as consisting "of fine transformation products with arbitrary orientations."

The scarcity of detailed information on the structure of adiabatic shear bands and the recommendations of the National Materials Advisory Board report on dynamic deformation[8] motivated the investigation whose results are reported herein. Titanium and Ti-6 pct Al-4 pct V alloy were chosen because they are target materials and they are known to form adiabatic shear bands upon impact.

H. ANDREW GREBE, formerly Graduate Student, Department of Metallurgical and Materials Engineering, New Mexico Institute of Mining and Technology, Socorro, NM 87801, is Works Metallurgist, Tubemakers of South Africa Ltd. Pty., Box 1905, Vereeniging 1930, South Africa. HAN-RYONG PAK, Assistant Professor, Department of Metallurgical and Materials Engineering, and MARC A. MEYERS, Associate Director, Center for Explosives Technology Research, are with New Mexico Institute of Mining and Technology, Socorro, NM 87801.

Manuscript submitted March 23, 1984.

II. EXPERIMENTAL TECHNIQUES AND MATERIALS

A. *Projectiles and Gun*

Cylindrical projectiles with a "stepped" front portion, mounted in polypropylene sabots, were used. They were made of steel (1.22 pct C, 0.21 pct Mn) in the quenched condition, yielding a hardness HRC 50-60. Figure 1(a) shows the projectile and sabot, separately, on the left-hand side, and the mounted position, on the right-hand side. The outside diameter was 10.5 mm and the step diameter was 3 mm. "Stepped" projectiles were introduced by Wingrove.[20] The step establishes a fixed amount of shear (at the step) constant for various degrees of penetration. Hence, the strain rate, at a fixed strain, can be varied independently by varying the projectile velocity.

The projectiles, mounted in the sabots, were fired from a 0.6 caliber (15 mm) smooth bore cartridge gun; the Mann barrel was 1.52 m long and was fixed in a Mitchell mount. A 20 mm breach was used, and the cartridges were fired by percussion action of a 115 V generator source using a sequencer detonation box. Improved military rifle (IMR 4895) powder was used to accelerate the projectiles. The powder charge was measured into a 20 mm diameter cartridge.

The projectile velocity was determined by measurement of transit times over a fixed distance with flash radiography. The Hewlett Packard three channel (115 kV) system consisted of three X-ray tubes perpendicular to the projectile trajectory. Two of these tubes were parallel. A time delay generator in the system pulsed each tube at a preset time; delays could range from 30 μs to 300 μs. The time delay generator was triggered when the projectile passed through a copper wire grid. A radiograph from the two parallel tubes is shown in Figure 1(b). To a first approximation (parallax and other corrections have to be made in a rigorous calculation), the velocity can be found by dividing the distance D (Figure 1(b)) by the difference in delay times; each image on Figure 1(b) comes from one tube. In the example case, D was equal to 112.5 mm (prior to photograph size reduction), and the delay difference was 133 μs. This yields a velocity of 846 m per second. The angles of the trajectory with the vertical and horizontal projections of the projectile axis were also determined. These angles varied between 0 and 2 deg for the different experiments assuring a fairly normal impact of the projectile on the target.

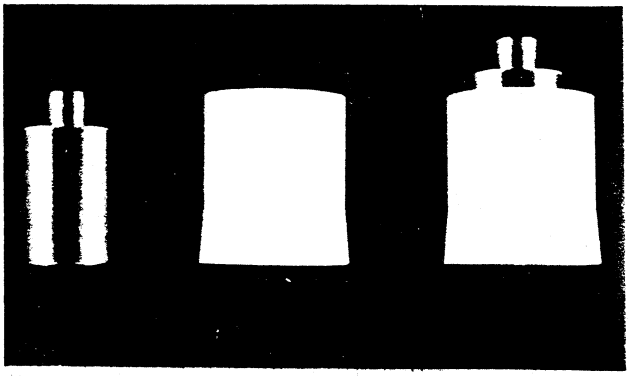

(*a*)

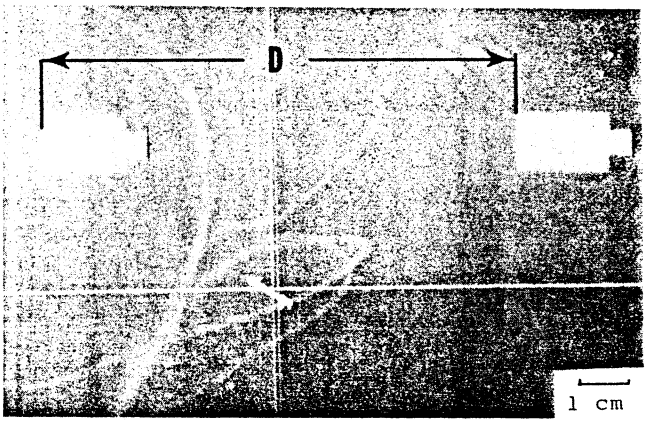

(*b*)

Fig. 1—(*a*) Projectile and polypropylene sabot viewed separately (left) and in mounted position (right). (*b*) Radiographs of projectile in free flight.

B. *Targets*

The targets (100 × 100 × 12.5 mm) were clamped at a distance of 40 cm of the barrel end and in such a way that the surface was perpendicular to the barrel axis. Target and projectile fragments could be recovered, in the case of total perforation, by means of a fiberboard recovery pack placed behind the target. The titanium (commercial grade II) and Ti-6 pct Al-4 pct V (hereafter named Ti 6 Al 4V) were purchased as 12.5 mm thick plates. Chemical analysis revealed the following elements: Ti (0.62 pct C, 0.04 pct Fe, 0.012 pct N, 0.13 pct O); Ti 6 Al 4V (0.03 pct C, 0.16 pct Fe, 6.2 pct Al, 4.0 pct V). The titanium plates were annealed in Sentri-Pak bags at 800 °C for one hour; the resultant microstructure was α (hcp). The grain size, as measured by the linear intercept method, was 61 μm.

The Ti 6 Al 4V plates were annealed at 800 °C for one hour in Sentri-Pak bags; the resultant structure was a mixture of α (hcp) and β (bcc) phases. The resultant grain size, as measured by the linear intercept method, was 8 μm. The microindentation hardnesses of the annealed titanium and Ti 6 Al 4V plates were, respectively, HVN 170 and HVN 290.

C. *Microscopy*

Specimens were sectioned using a low speed Isomet saw and prepared for optical examination by standard techniques. Scanning electron microscopy was conducted in a Hitachi HHS-2 R unit. For transmission electron microscopy a Hitachi HU-200 F unit operated at 200 kV was used. Specimens were cut from the general deformation zone produced by impact and from shear band zones. Thin wafers (0.25 to 0.3 mm thick) were cut using a low-speed Isomet diamond blade. These wafers were further reduced to a thickness of less than 0.1 mm by grinding on silicon carbide paper. A Fischione jet electropolisher equipped with an auxiliary (cooling) bath was used to thin the 3 mm disks to perforation. For specimens in the shear band zone, one side of the foil was coated with "stop-off" to isolate a part of the

shear band and to ensure thinning in that area. The electrothinning solution consisted of a 0.5 vol pct HF, 3 vol pct H_2SO_4, and 96.5 vol pct CH_3OH; the recommended temperature was −40 °C and voltage was 25 V.

Microprobe analysis was conducted in a Cameca MBX unit operating at 15 kV: the data were reduced by the computer program ZAF of the Sandia Task; elemental scans were conducted for Si, S, Fe, Ni, and Cu. ZAF was developed by Sandia National Laboratories to obtain quantitative elemental analyses taking into account corrections for atomic number (Z), absorption (A), and characteristic fluorescence (F).

III. RESULTS AND DISCUSSION

A. *Ballistic Experiments*

The results of the ballistic impact experiments are shown in Table I. The pressures were calculated using the impedance matching technique.[21] The velocity range, 500 to 900 m per second, was chosen to produce a variation in penetration depth. It can be seen that the pressures generated in the target by impact are significant; one may expect substantial shock-wave induced defects on the substructural level from these pressures. Figure 2 shows the depth of penetration *vs* velocity. At 12.5 mm the target thickness was exceeded; this is indicated by the broken line in Figure 2. One may qualitatively understand better the concavity of Figure 2 if one considers that the kinetic energy of the projectile (proportional to the square of the projectile velocity) is transformed into deformation energy. The higher strength of the Ti 6 Al 4V alloy is responsible for the greater penetration resistance.

Figure 3(a) shows the projectile partially embedded in the target; one can see that the tip of the projectile underwent considerable erosion and that the step was only partially effective in concentrating the shear strains. Total perforation occurred for impact velocities of 766 and 846 m per second, for Ti and Ti 6 Al 4V, respectively. The mechanism of perforation is clearly of the plugging-type for Ti, and plugging and spalling for Ti 6 Al 4V. Backman[22] and Zukas *et al.*[23] describe in detail these mechanisms. Figures 3(b) and 3(c) show the back views and side views of the perforated targets and plugs formed. For Ti, a cylinder is ejected at the back surface, and the external surface of the cylinder evidences intense shearing. For Ti 6 Al 4V the back portion of the cylinder ejected has a cap; this cap is generated by a fracture induced by tensile stresses at the back surface of the target. This mechanism is called "spalling" and is described in greater detail by Meyers and Aimone.[24] Spalling is due to tensile pulses produced by shock waves reflecting at a free surface. The formation of the plug is thought to be due to adiabatic shear bands; the shearing at the plug-target interface during penetration is accomplished by the propagation of adiabatic shear bands.

B. *Optical Microscopy of Shear Bands*

Adiabatic shear bands were observed in all six targets. As expected, their number as well as length increased with projectile velocity. Figure 4 shows the cross-section of Ti-6Al-4V specimen after impact at 846 m per second. The cross-section was etched and shear bands are indicated by arrows. At higher magnifications a greater number of bands become evident. These bands were counted along the two sides of the cross-section (passing through the axis of the projectile); Figure 5 shows the variation of the number of shear bands per cross-section with impact velocity. The results displayed in Figure 5 should be considered to be qualitative but are useful as they show the dependence of shear band formation on projectile velocity; the number of bands observed in a diametral cross-section of the target was simply counted. No great difference in band numbers between Ti and Ti 6 Al 4V could be observed. Figure 6 shows the typical morphologies for the shear bands. The difference in grain size between Ti and Ti 6 Al 4V is readily observable. The measured shear-band widths varied between 1 and 10 μm for both Ti and Ti 6 Al 4V. It is interesting to notice that shear-band width seems to be independent of projectile and/or target size. In this investigation, the variation in thickness is at least partially due to the angle between the free surface plane and the shear-band plane. The observed thickness is minimum for normality between the two planes. The shear bands propagate in a transgranular mode in titanium, while in Ti 6 Al 4V their width is about the same as the grain size. Upon etching, the bands exhibited a rough,

Table I. Ballistic Impact Experiments

Material	Velocity (m/s)	Pressure (GPA)
Ti	578	8.0
Ti	608	8.4
Ti	766	11.0
Ti6Al4V	556	7.8
Ti6Al4V	640	9.0
Ti6Al4V	846	12.1

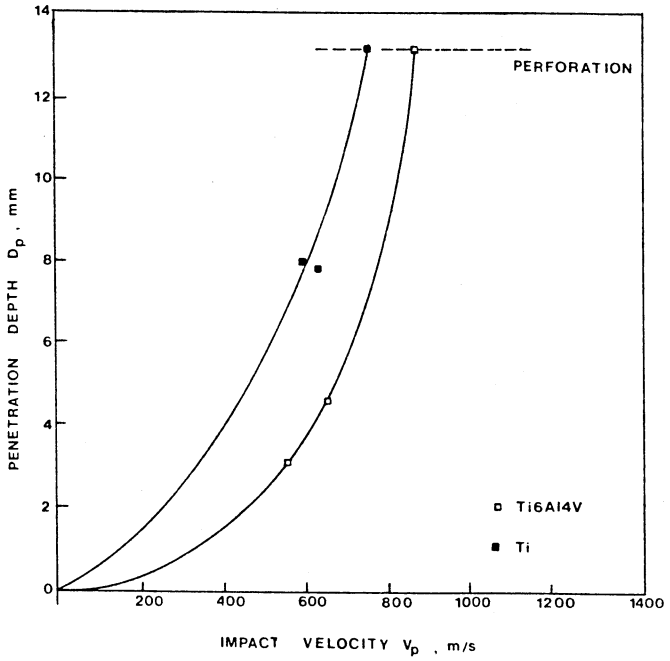

Fig. 2—Plot of depth of penetration (D_p) *vs* velocity of projectile (V_p).

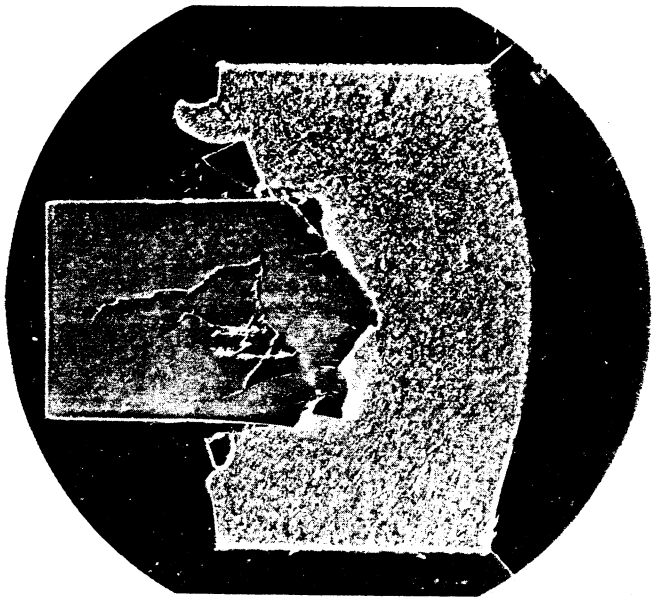

(*a*)

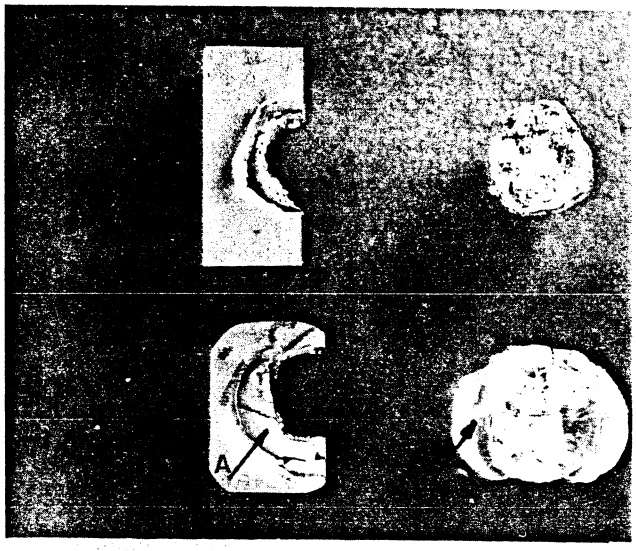

(*b*)

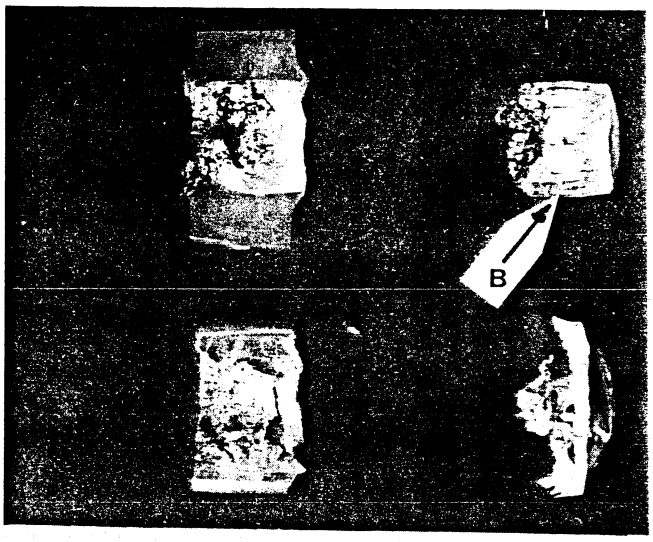

(*c*)

Fig. 3 — (*a*) Cross section of projectile and target showing partial penetration. (*b*) Back view of target showing spalling/plugging of back surface of Ti6Al4V (bottom) and plugging of titanium (top) targets. (*c*) Side view of target showing spalling/plugging of Ti6Al4V (bottom) and plugging of titanium (top) targets.

irregular surface in titanium and a smooth appearance in Ti 6 Al 4V. The bands tended to propagate along the mid plane of the target in Ti 6 Al 4V within banded zones referred to as "hatching" by Woodward[26] and Me-Bar *et al.*,[27] who found the same predisposition for shear-band propagation along these "hatched" regions for similar alloys. Hatching is probably due to segregation and subsequent rolling: fluctuations of mechanical response may account for the preferential shear band propagation along the hatched zone. The band will propagate preferentially in a region where (a) the resistance to plastic deformation is lower: and (b) the predeposition for band formation is higher. In Figure 6(b) the banding of the structure parallel to the shear band (marked by arrow) is the result of "hatching".

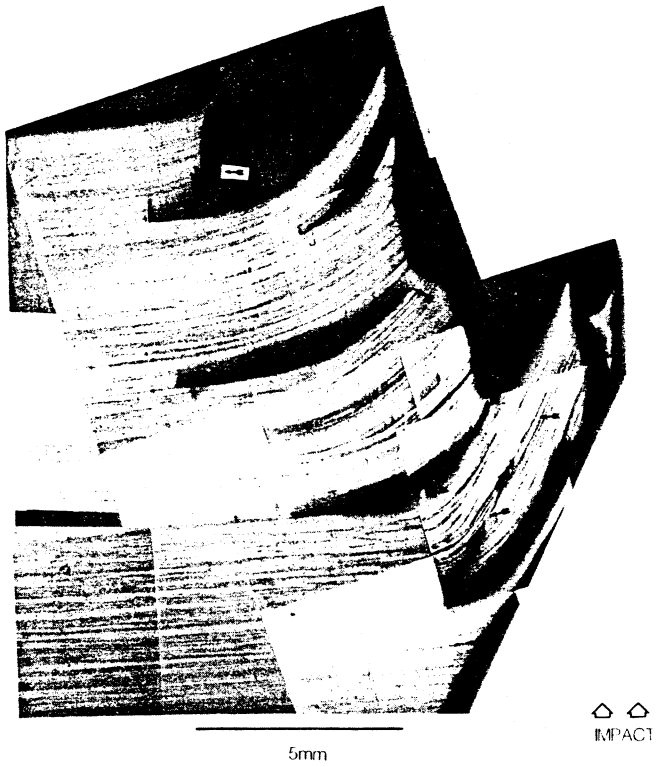

Fig. 4 — Cross section of Ti6Al4V target impacted at 846 m/s after polishing and etching; shear bands are marked by arrows.

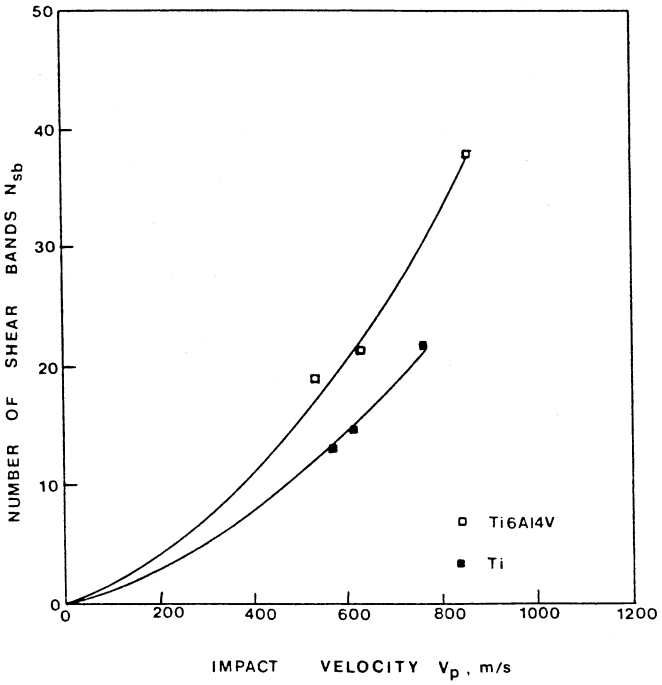

Fig. 5 — Plot showing number of shear bands (N_{sb}) observed in target cross section *vs* velocity of projectile (V_p).

In many instances the pattern of propagation of shear bands was irregular, with shear bands intersecting each other. Such an event is depicted in Figure 7; band 1 was formed first, and later sheared by band 2. One can use the

(*a*)

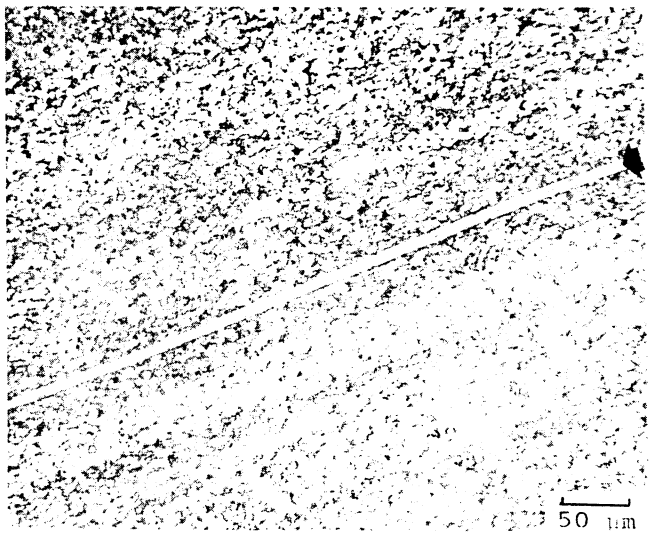

(*b*)

Fig. 6 — Shear bands arrowed in (*a*) titanium and (*b*) Ti6Al4V.

height of the shear step T and the thickness of the band t to estimate the amount of shear in the band. One finds an engineering shear strain of 15. Shear strains as high as 572 were reported by Moss;[27] hence, large shear strains are a prominent feature of adiabatic bands.

Figure 8 shows the onset of fracture along the shear bands. Voids or elongated cavities were found in both titanium and Ti 6 Al 4V. The cavities were spherical until their diameter reached the thickness of the shear bands; from there on, void coalescence and extension along the shear band resulted in the elongated cavities. Winter[28] and Me-Bar and Shechtman[19] observed similar features. However, it is only by applying the concept of nucleation, growth, and coalescence of voids occurring in spalling that one can understand the formation of these voids in the shear band region. The phenomenon is highly localized in this case because the threshold stress for void nucleation is much

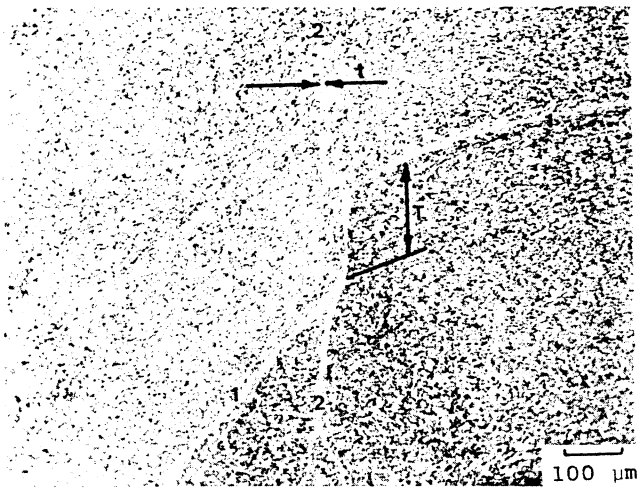

Fig. 7—Shear band intersection in Ti6Al4V. t is the band thickness and T is the offset at shear-band intersection.

lower. The sphericity of the voids (until their diameter is equal to the band thickness) indicates that the material has high ductility. This preferential nucleation is caused by the higher temperature inside the shear band, with an attendant flow stress decrease. Erlich *et al.*[7] found that lack of tensile stresses after impact (or detonation) resulted in only bands; no voids were observed, leading them to conclude that they are due to the tensile stresses. Rogers,[3] on the other hand, proposed two explanations for the voids: (a) tensile forces (the one corroborated by Erlich *et al.*[7]); (b) growth by cavitation within a heated zone during deformation, atomic mobility at high temperature being responsible for the formation of the spherical voids to reduce surface energy.

The projectiles also showed profuse adiabatic shear bands; their arrangement and morphology were quite different than in the targets. The bands showed the characteristic "white etching"[3] appearance and formed a complex interconnecting pattern. This is shown in Figure 9(a). The band indicated by 1, 2, 3 seems to have formed first, transversal bands forming later and establishing steps. Since the projectile is brittle and the pattern of the bands is so irregular, one could speculate that the projectile fragments at the impact interface and that molten metal flows within the crack openings rewelding the projectile. In band 4 (Figure 9(a)) one can see little evidence of shear; however, the band is white. Figure 9(b) shows a section of the projectile embedded in a nickel target; one can clearly see the fragmentation. Electron microprobe scans were made across the white bands in the positions marked in the photomicrograph. No nickel could be detected in any of the scans inside the projectile, discarding the hypothesis that interfacial melting occurred and that liquid metal (a mixture of nickel and iron) would have been injected into the fractured projectile, resolidifying. The composition across the shear bands did not show any inhomogeneities.

The results of the microindentation hardness measurements (each bar represents ten measurements) are shown in Figure 10. For titanium and Ti 6 Al 4V the hardness in the band was not substantially different from the surrounding region. This is in accord with Me-Bar and Shechtman's[19] results for Ti 6 Al 4V but in disagreement with Winter's[28] results for titanium; he found a substantially higher hardness inside the bands. In the steel projectile, the hardness inside the bands was lower than the surrounding regions. This is in contrast with previous findings for steel. However, the observations reported in the literature[3] refer to regular shear bands and not "islands" as the ones observed in the projectile. An AISI 1040 target, in the quenched and tempered condition, was also subjected to impact. Adiabatic shear bands were observed to form, and their hardness was higher than the matrix. This shows that the white "islands" within the projectiles are different from the conventional bands, and that the cooling rate and forming conditions could be very different.

For the three cases the hardness in the matrix increases as the shear band is approached. This is due to work hardening induced by diffuse deformation surrounding or preceding the localized shear localization phenomenon.

C. *Fractography*

Fracture manifested itself primarily in two modes: (a) spalling induced by tensile pulses generated by the reflection of the shock wave at the back surface of the target; and (b) shear/tensile failures propagating along shear bands.

Figure 3(b) shows the back side of the targets. Spalling is evident in the specimen marked with an arrow A. It precedes the perforation, since the shock wave propagates in titanium at a velocity of ~5000 m per second, while the impact/penetration velocity is lower by roughly one order of magnitude. Hence, spalling has already taken place when the projectile "plugs" through the target. Figure 11 shows a scanning electron micrograph of the spall surface in Ti 6 Al 4V. The characteristic "dimpled" appearance can be seen, showing that this alloy does not lose its ductility at these extreme strain rates.

The observation of the fracture along the internal plug surface (marked with arrow B in Figure 3) was more difficult. Direct observation along the plug surface did not reveal any features (except for shear striations). Observations of the cracks inside the shear bands were therefore conducted. Figure 12 shows a shear band terminating at a crack. Figure 13(a) shows the impact region and the band direction (hatched line). A saw-cut was made to release the opened portion of the band without introducing additional deformation. Figures 13(b), 13(c), and 13(d) show closer views of the fracture surface, generated when a shear band was subjected to tensile stresses. The morphology does not resemble any conventional fracture surface. One observes "geometric protrusions" in Figure 13(c); the other area of Figure 13(b), a smooth surface, is shown in Figure 13(d). Spherical voids can be seen in these surfaces. The sequence of formation of the crack as it is envisioned is shown in Figures 13(e) and (f). The shear band material, upon cooling, must be more brittle than the matrix (compare Figure 13 and Figure 11). Upon tensile stressing, fracture must occur along the interfaces, with portions staying with one side and portions with the other side. This leads to the pattern observed in Figure 13(b). Another possibility for the cracks is melting, solidification, and contraction along the band. The contraction would lead to cracking if the rapidly-solidified material is very brittle.

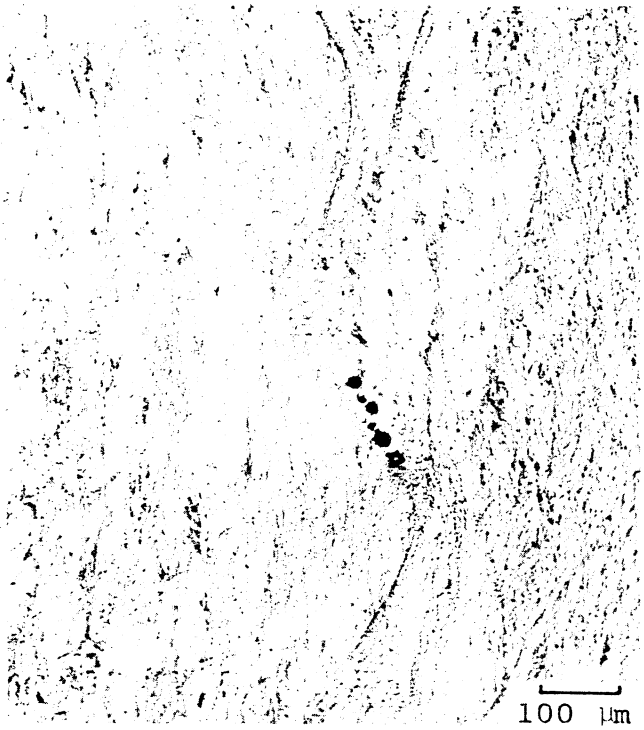

(*a*)

(*b*)

(*c*)

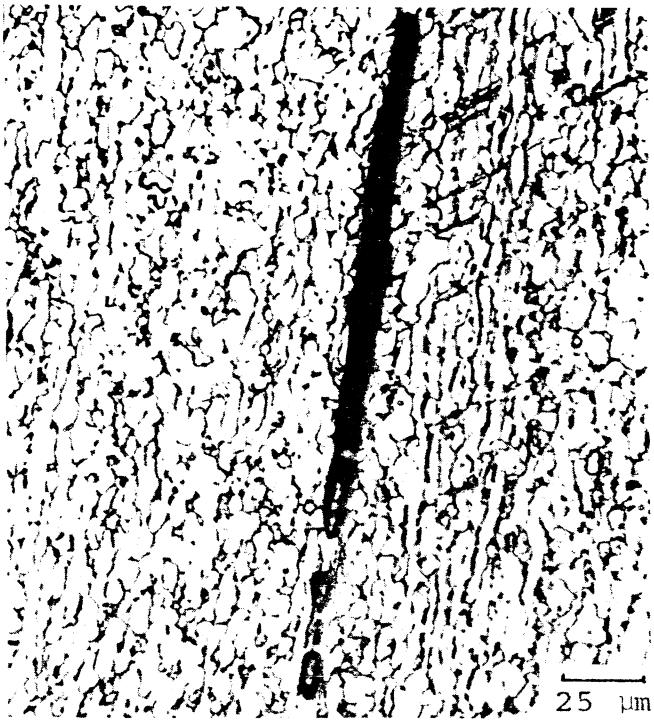

(*d*)

Fig. 8 — Voids (*a*) and blunted cracks (*b*) in titanium; voids (*c*) and blunted cracks (*d*) in Ti6Al4V.

(*a*)

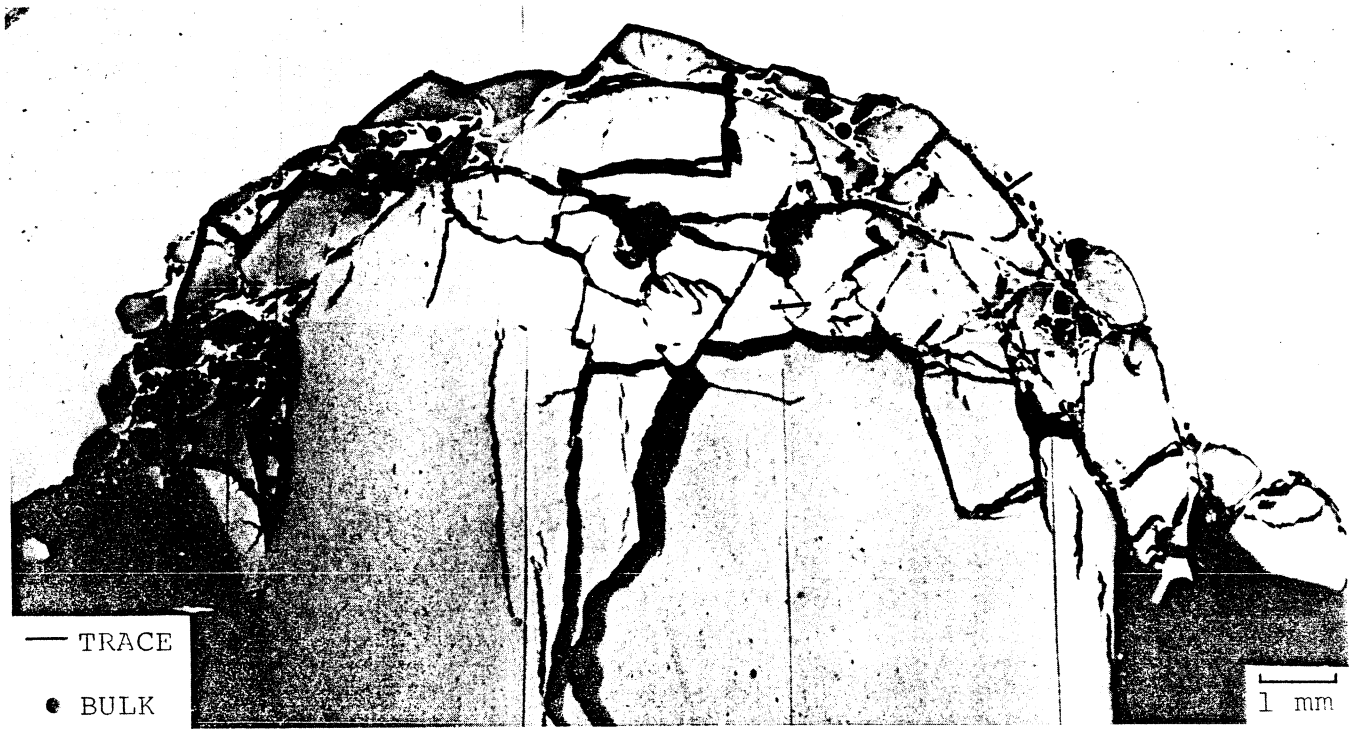

(*b*)

Fig. 9—(*a*) Shear bands and "islands" in projectile. (*b*) Sectioned projectile showing "bands" where electron microprobe scans were made.

(*a*)

(*b*)

(*c*)

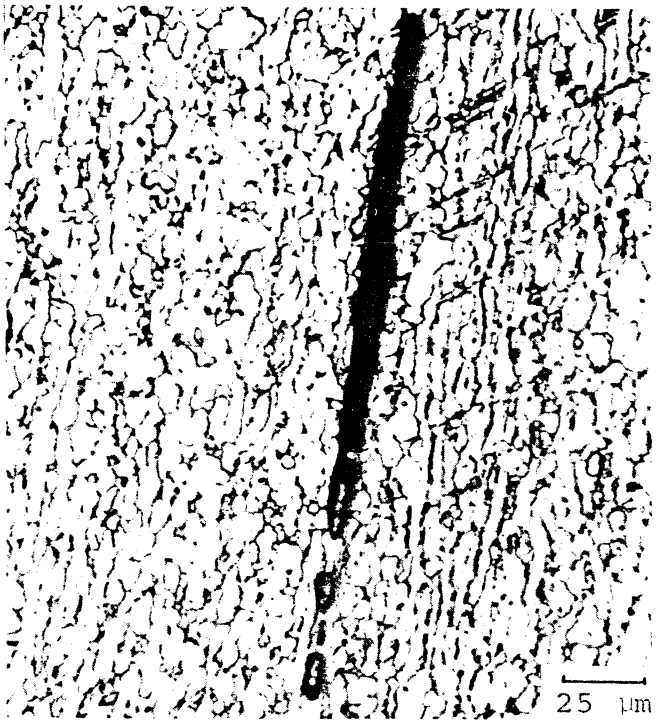

(*d*)

Fig. 8 — Voids (*a*) and blunted cracks (*b*) in titanium: voids (*c*) and blunted cracks (*d*) in Ti6Al4V.

(*a*)

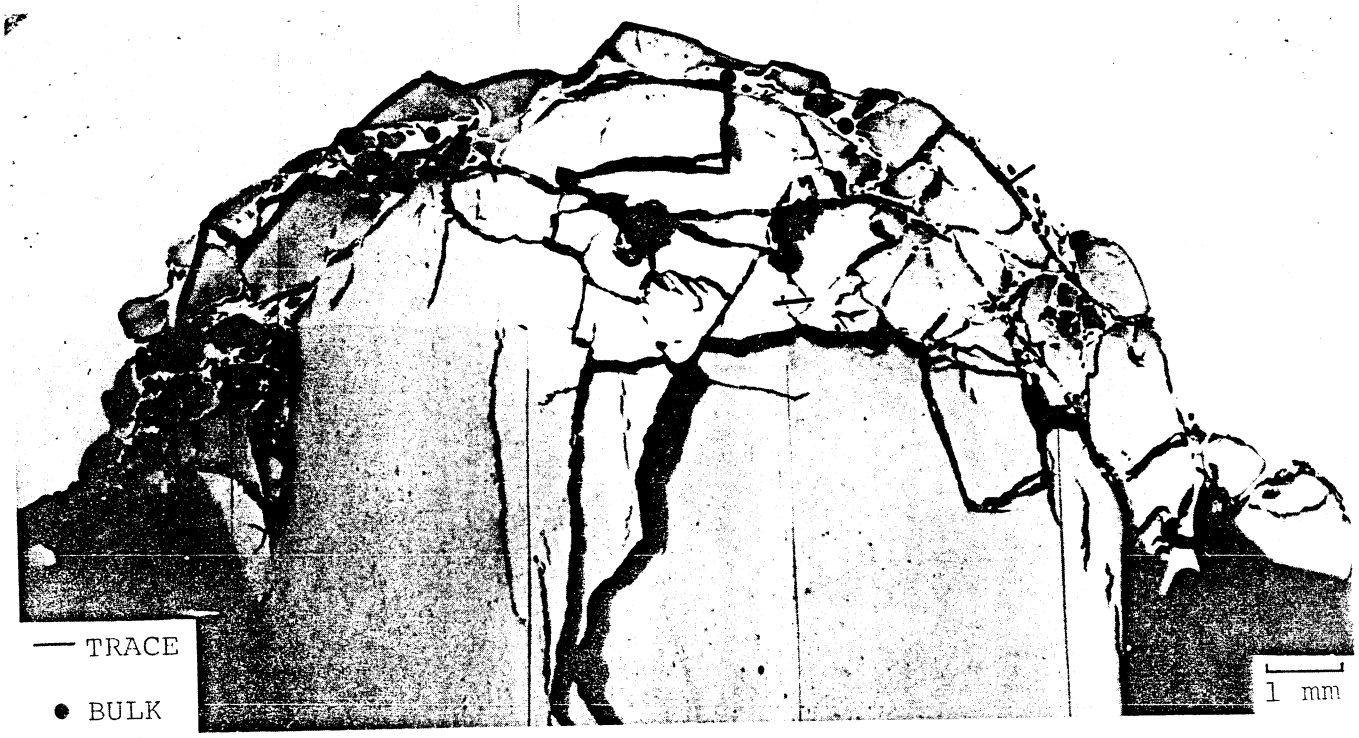

(*b*)

Fig. 9—(*a*) Shear bands and "islands" in projectile. (*b*) Sectioned projectile showing "bands" where electron microprobe scans were made.

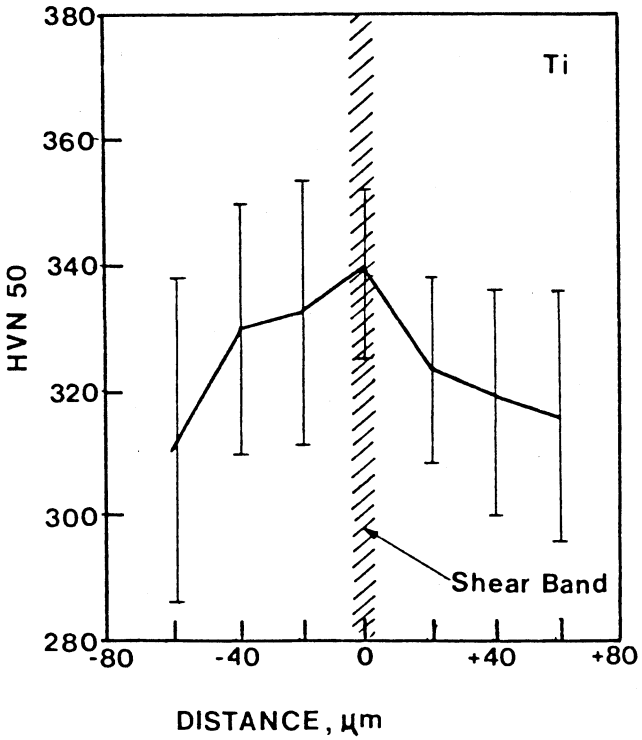

(*a*)

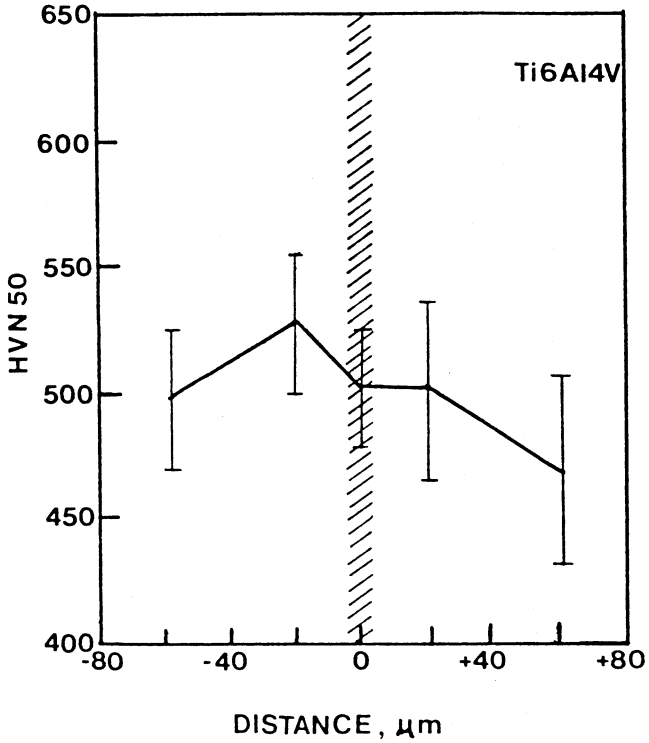

(*b*)

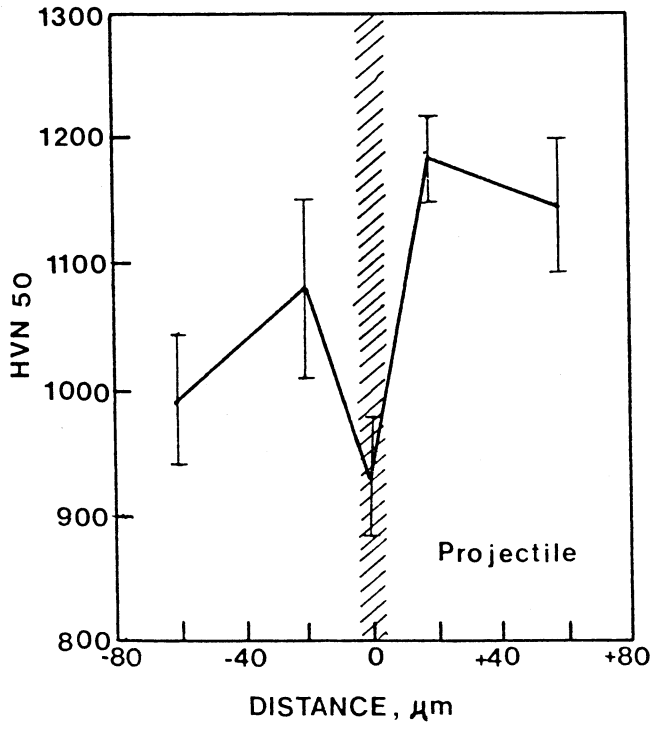

(*c*)

Fig. 10—Vickers microindentation traverses for (*a*) titanium, (*b*) Ti6Al4V, and (*c*) projectile.

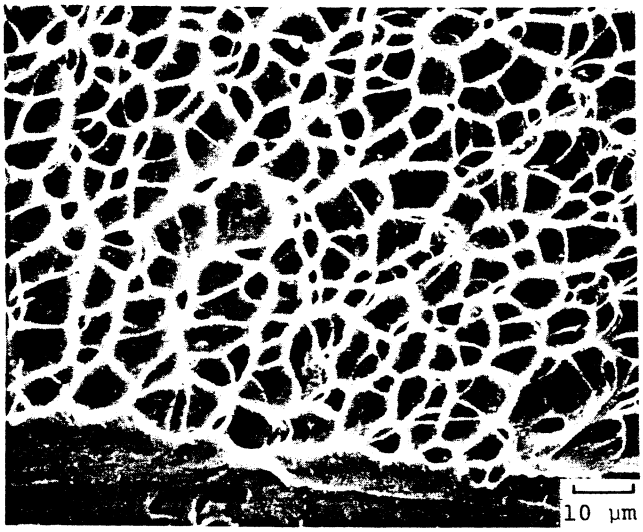

Fig. 11—Characteristic dimples observed in spall region of Ti6Al4V.

Figure 14 shows the morphology of the fracture inside a band in titanium. One sees regions resembling the ones in Figure 13 (Figure 14(b)) and regions with dimpled morphology typical of titanium (Figure 14(a)). Unique fracture features were also observed by Stock and Thompson[14] and Manion and Wingrove;[29] they called these features "knobbles" and suggested that these features could be due to localized melting. Rogers[3] proposed a mechanism for this "knobbly" fracture by which conventional ductile fracture occurs and is followed by heat generation by friction of the opposing surfaces.

D. *Transmission Electron Microscopy*

The impact of the projectile against the targets creates (a) a deformation region of a generalized nature and (b) zones of intense shear.

In the generalized deformation region one has deformation by means of plastic wave propagation. The defect density increases as the impact surface is appoached. Specimens exhibited a characteristic high dislocation density with

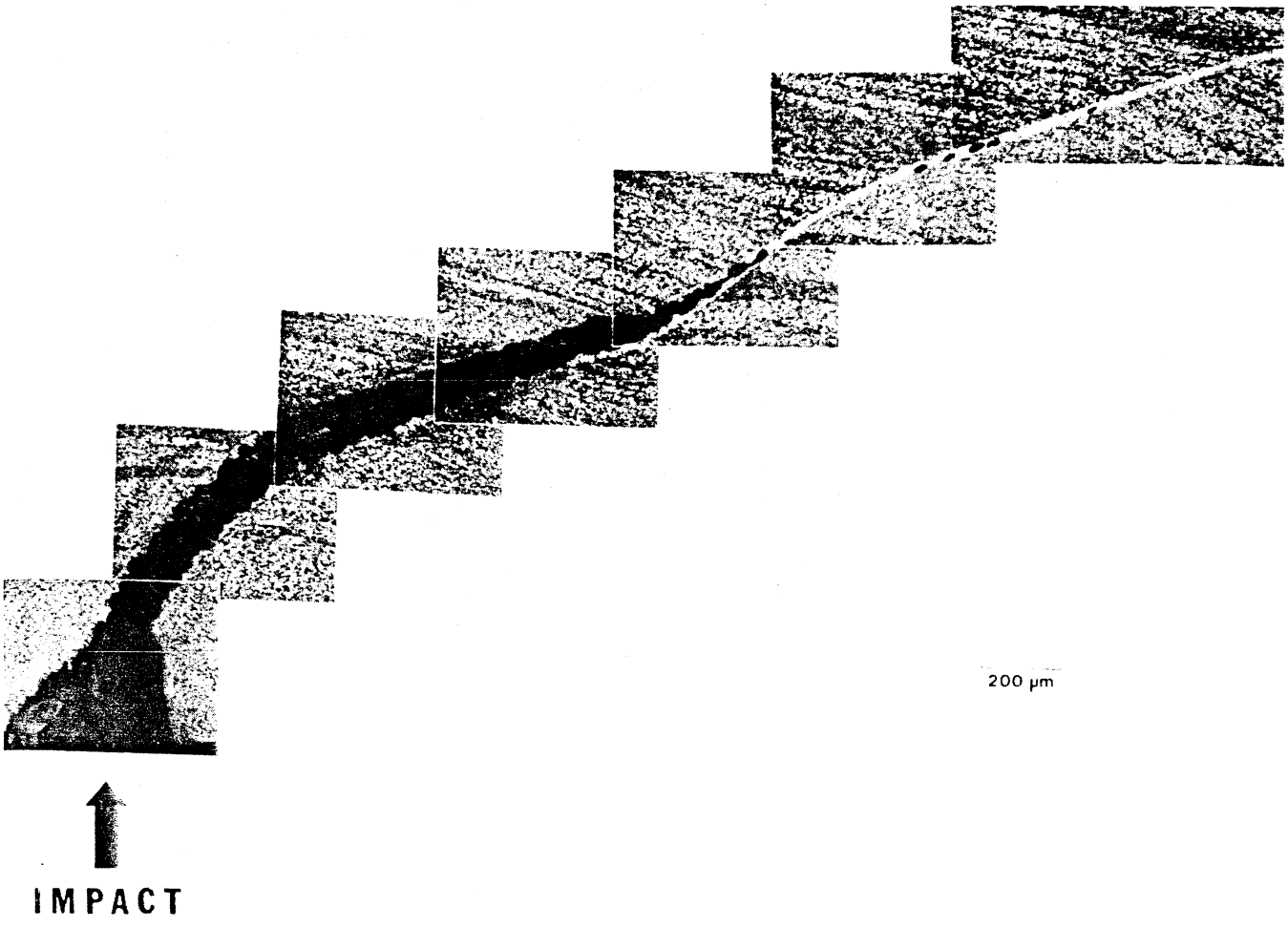

Fig. 12—Shear-band crack propagating from the impact surface in Ti6Al4V.

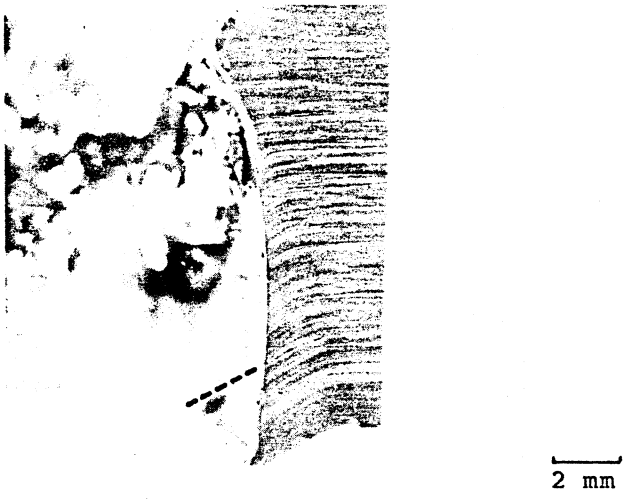

(a)

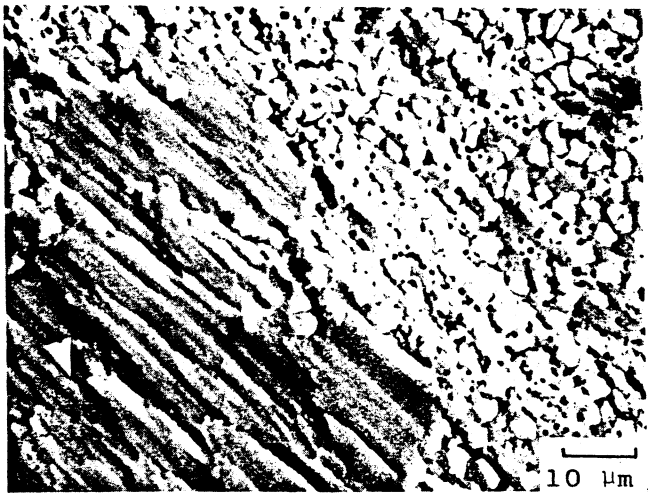

(b)

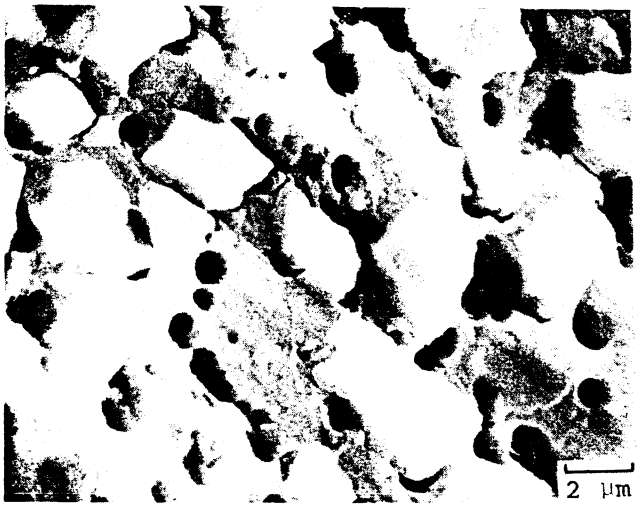

(c)

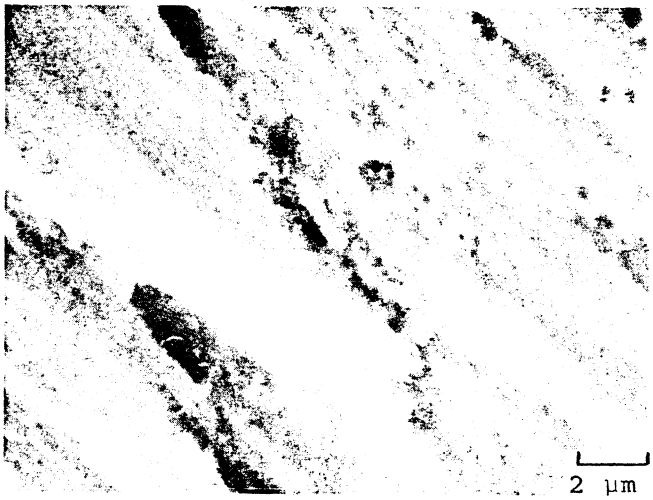

(d)

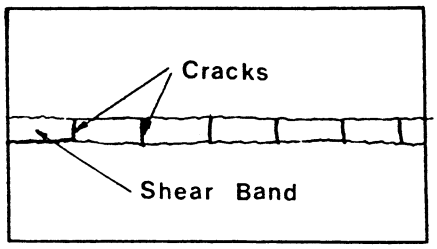

(e)

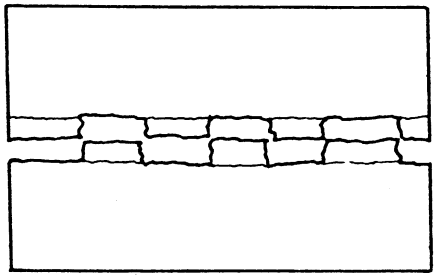

(f)

Fig. 13—Fractographs of shear-band cracks in Ti6Al4V. (*a*) Shear-band crack that was observed; (*b*) morphology of crack surface shown by SEM; higher magnification scanning electron micrographs of (*c*) "knobbly" and (*d*) smooth region; (*e*) and (*f*) proposed sequence for the formation of the "protrusions".

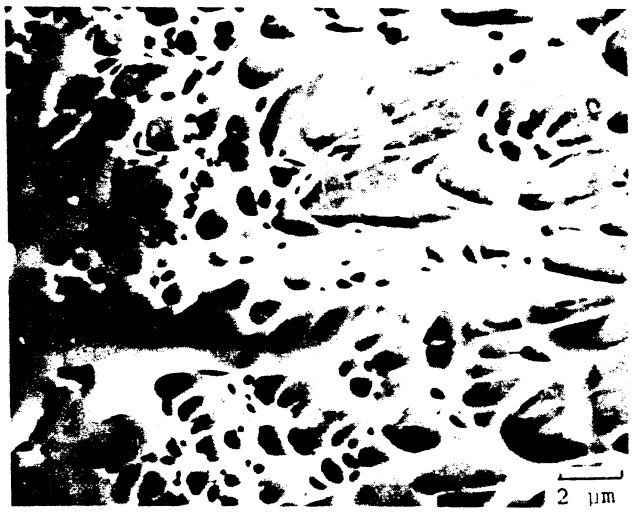

(*a*)

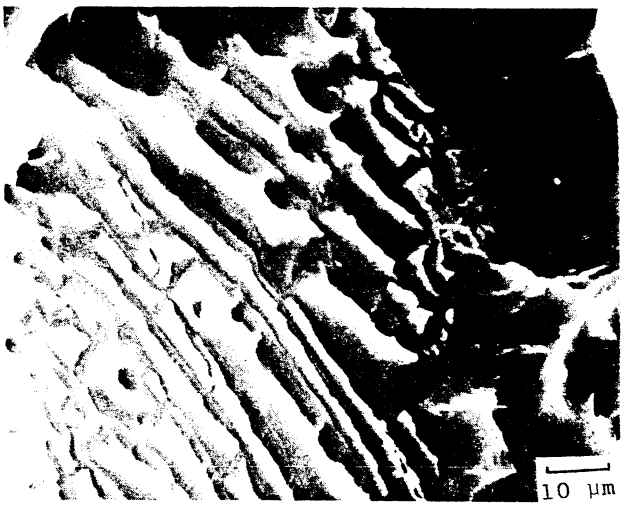

(*b*)

Fig. 14—Fractographs of shear-band crack in titanium: (*a*) conventional dimpled region and (*b*) "knobbly" region.

twinning. Figures 15 and 16 show typical substructures for titanium and Ti 6 Al 4V in areas away from shear bands. For titanium (Figure 15), a random distribution of dislocations and bands was observed. Traces of the bands seen in Figure 16 were parallel to $\{1\bar{2}11\}$, and thus these structures are considered to be deformation twins; such deformation twins were also observed by Koul and Breedis.[30]

For the Ti 6 Al 4V alloy, two different substructures were observed; while the α (hcp) phase showed dislocation arrays and profuse twins parallel to $\{1\bar{2}11\}$ and $\{0\bar{1}11\}$ similar to the ones in titanium, the β (bcc) phase showed arrays of straight parallel dislocations. These linear dislocation arrays resemble the ones observed after shock loading iron. In iron these straight dislocations have been identified as screw dislocations, which exhibit a reduced mobility at low temperatures and high strain rates. The montage of Figure 16 shows both the α and β phases, and the differences are clearly evident. The region indicated A is α (hcp) phase while B is β (bcc) phase.

Fig. 15—Substructure produced by impact in titanium.

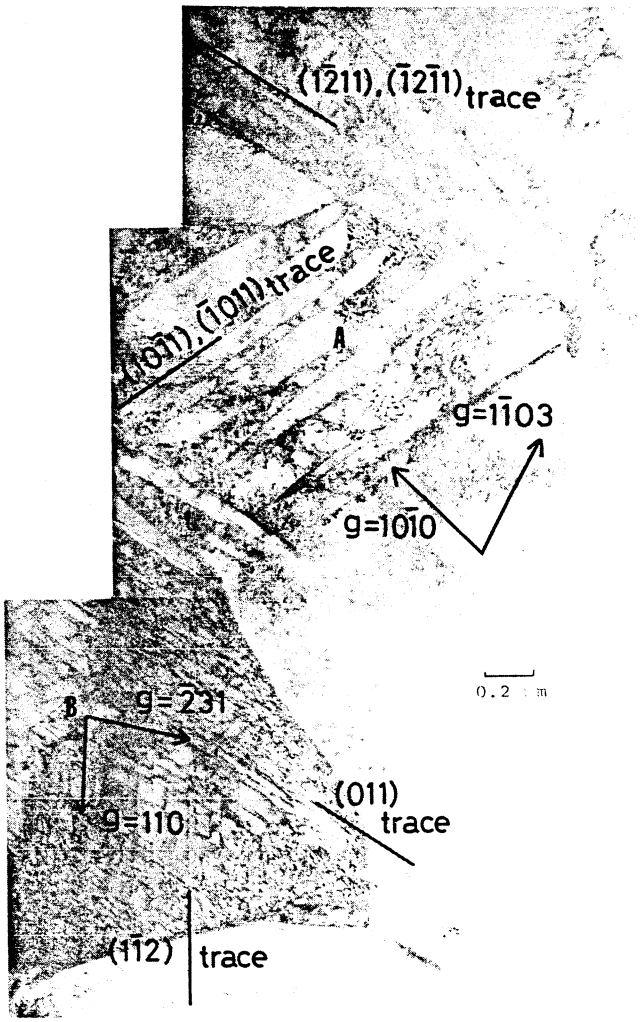

Fig. 16—Impacted microstructures Ti6Al4V showing two distinct areas: (A) α-hcp; (B) β-bcc.

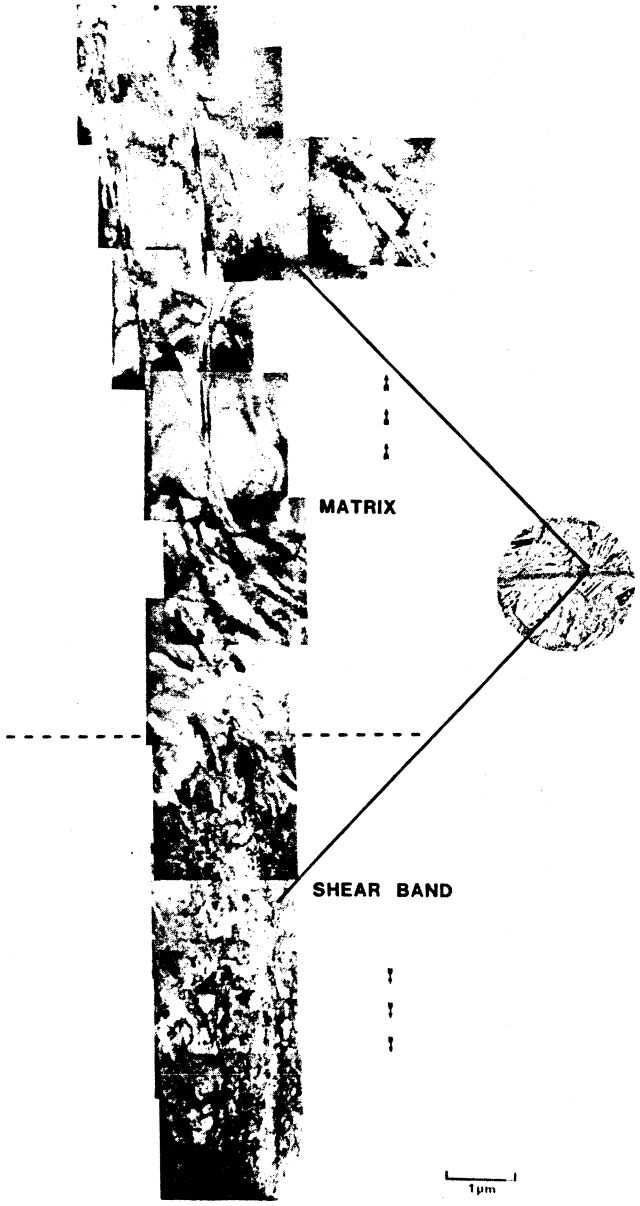

Fig. 17—"Montage" showing transition from large grains to microcrystalline features within shear band.

The substructures of a shear band and adjacent regions are shown in the montage of electromicrographs in Figure 17; the optical micrograph indicates the microstructures of the areas observed. The shear band consists of small "mosaic type" features, compared with the larger grained matrix. Detailed examination of the shear band by electron diffraction showed both a ring and a spot pattern. The ring pattern, shown in Figure 18(c), was taken from area A (large square) in Figure 18(a). This pattern could be indexed as hcp structure by using lattice parameters (a = 2.95 A, c = 4.68 A) of pure titanium. Arcing of the spots in the pattern is not asterism as usually seen when heavy deformation takes place, but rather indicates a multitude of micrograins. Diffraction rings have been known to be produced if the size of grains is extremely fine ($\ll 1$ μm).[31] The presence of such fine grains is evident in the dark-field micrograph of Figure 18(b), obtained by using the spot circled in Figure 18(c). Fine, bright areas in the micrograph reveal grains; their size is in the range of 0.3 μm. These fine grains exhibit some preferred orientation; the diffraction pattern taken from a small area, framed by B in Figure 18(b), shows one single orientation of the hcp structure. It should also be noticed that the boundaries of these fine grains are irregular and not very well defined.

Thus a single crystallographically oriented microcrystalline structure exists for the shear band in titanium. Lattice distortions of up to 60 deg may have occurred in the shear band; shear band rotation may have occurred causing some preferred orientation. If recrystallization then occurred, this may partly account for the "messy" grain boundaries observed in the band.

The area very close to the shear band consisted of dislocation debris, and the bright-field micrographs in Figure 19 showed evidence of twinning, considered to having been formed during impact. Trace analysis indicated twins along the $(1\bar{2}1\bar{1})$ (or $(\bar{1}\bar{1}21)$) and $(0\bar{1}11)$ planes.

IV. CONCLUSIONS

The formation of adiabatic shear bands and of impact-induced fracture was studied in titanium and Ti-6Al-4V alloy. Distinct regions of strain concentration were identified and were found to have an important effect on subsequent fracturing. The microindentation hardness of the bands was not significantly different from the bulk material. Observation of the fracture surfaces by scanning electron microscopy revealed unique features which were interpreted in terms of the modification of the mechanical properties inside the band region. Transmission electron microscopy was conducted in the general deformation region (produced by the projectile impact) and in the shear band. The dislocation/twin substructure in the general deformation region is that characteristic of shock-loaded titanium.[30] The microstructure of the shear band region revealed features that can be described as microcrystalline, with varying amounts of dislocations in the micrograins (0.3 μm diameter).

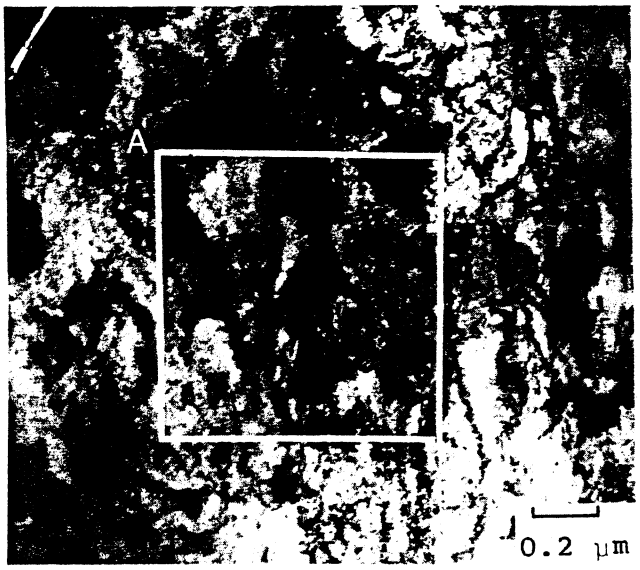

(*a*)

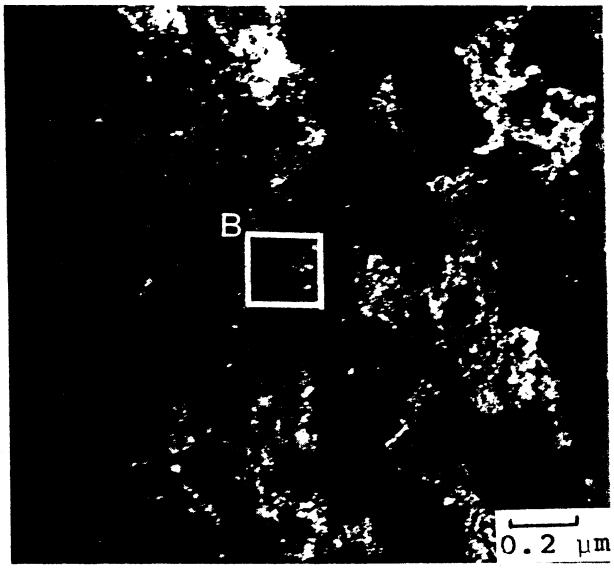

(*b*)

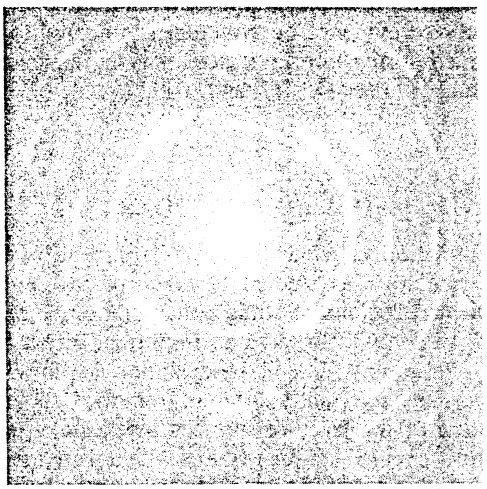

(*c*)

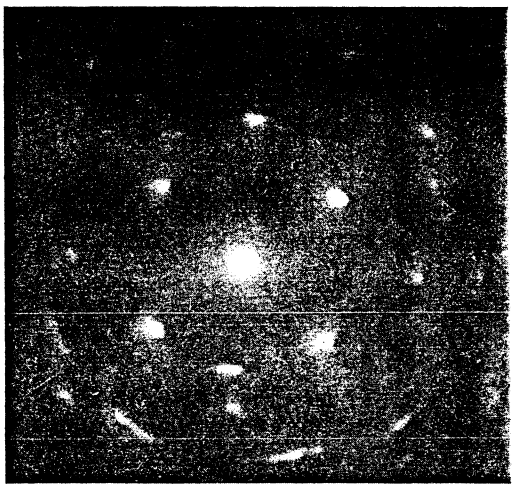

(*d*)

Fig. 18—Microcrystalline features observed within shear band in titanium: (*a*) bright field; (*b*) dark field of the same region as in (a) by a spot circled in c; (*c*) diffraction pattern of A (rings were indexed as $(1\bar{1}00)$, (0002), $(1\bar{1}01)$, $(1\bar{1}02)$, $(2\bar{1}\bar{1}0)$, $(2\bar{1}\bar{1}1)$, $(2\bar{2}00)$, and $(2\bar{2}02)$); (*d*) diffraction pattern of B. Foil plane is nearly parallel to $(01\bar{1}1)$.

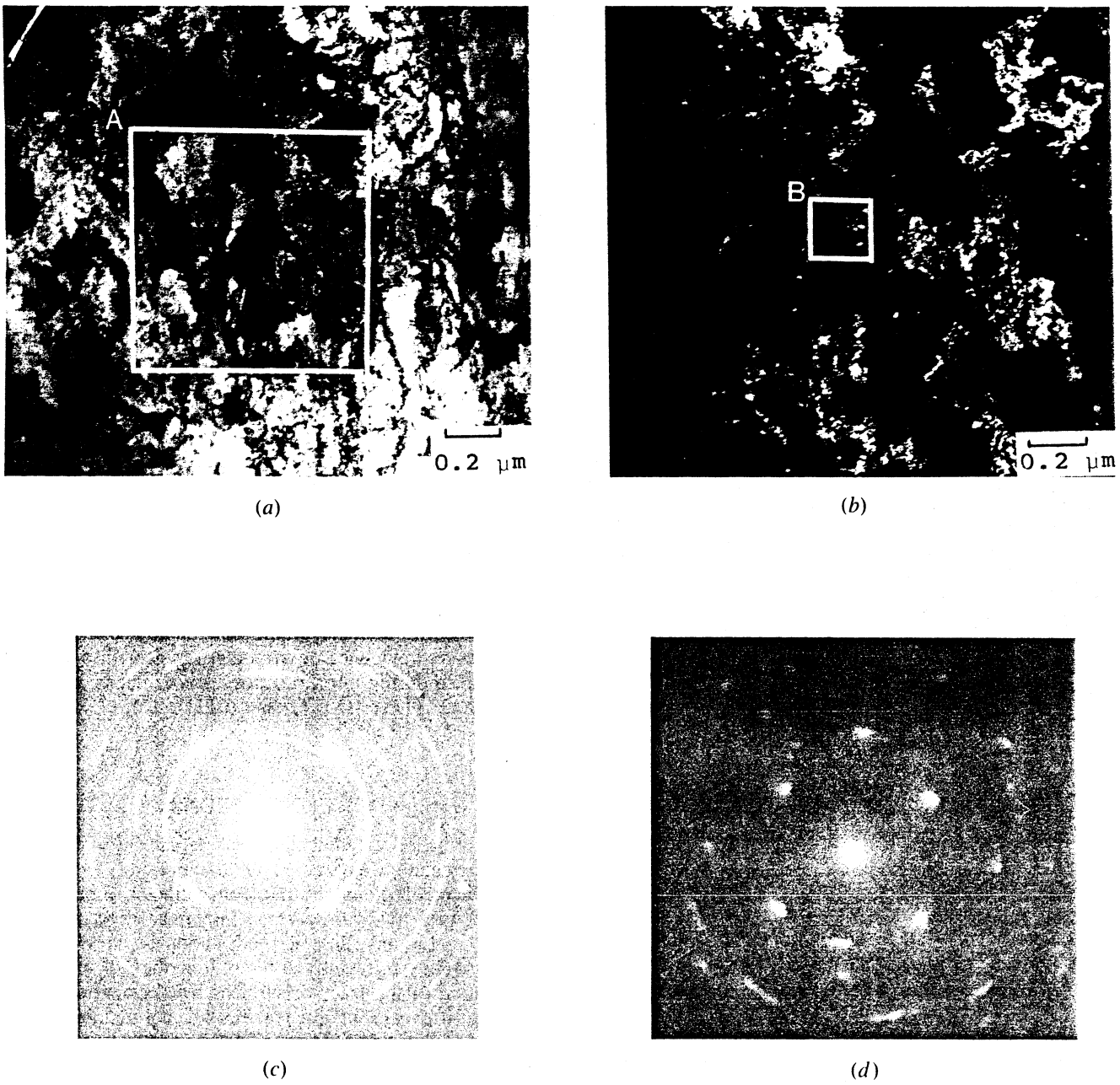

(*a*) (*b*)

(*c*) (*d*)

Fig. 18—Microcrystalline features observed within shear band in titanium: (*a*) bright field; (*b*) dark field of the same region as in (a) by a spot circled in c; (*c*) diffraction pattern of A (rings were indexed as $(1\bar{1}00)$, (0002), $(1\bar{1}01)$, $(1\bar{1}02)$, $(2\bar{1}\bar{1}0)$, $(2\bar{1}\bar{1}1)$, $(2\bar{2}00)$, and $(2\bar{2}02)$); (*d*) diffraction pattern of B. Foil plane is nearly parallel to $(01\bar{1}1)$.

Fig. 19 — Appearance of twin variants and dislocation debris in titanium in an area close to the shear band. Foil plane is nearly parallel to (01$\bar{1}$0).

ACKNOWLEDGMENTS

This research was supported by National Science Foundation Grant DMR 8115127 and by the Research and Development Division of New Mexico Tech. Dr. A. D. Romig, Sandia National Laboratories, provided invaluable help through discussions and by performing the chemical analysis of the materials and the electron microanalysis. The support provided by Mr. D. Collis and the TERA staff is gratefully acknowledged.

REFERENCES

1. G. B. Olson, J. F. Mescall, and M. Azrin: in *Shock Waves and High-Strain-Rate Deformation of Metals: Concepts and Applications*, M. A. Meyers and L. E. Murr, eds., Plenum Press, New York, NY, 1981, p. 221.
2. A. J. Bedford, A. L. Wingrove, and K. R. L. Thompson: *J. of the Austr. Inst. of Metals*, 1974, vol. 19, p. 61.
3. H. C. Rogers: *Ann. Rev. Matls. Sci.*, 1979, vol. 9, p. 283.
4. C. Zener and J. H. Hollomon: *J. Appl. Phys.*, 1944, vol. 15, p. 22.
5. R. F. Recht: *J. Appl. Mech. (Trans. A.S.M.E.)*, 1964, vol. 31, p. 189.
6. R. S. Culver: in *Metallurgical Effects at High Strain Rates*, R. W. Rohde, B. M. Butcher, J. R. Holland, and C. H. Karnes, eds., Plenum Press, New York, NY, 1973, p. 519.
7. D. C. Erlich, D. R. Curran, and L. Seaman: "Further Development of a Computational Shear Band Model", Report AMMRC TR 80-3, SRI-International, Menlo Park, CA, 1980, p. 51.
8. R. F. Clifton: in *Materials Response to Ultra-High Loading Rates*, W. Herrmann, ed., NMAB-356, National Academy of Sciences, 1980, p. 129.
9. Y. L. Bai: in source cited in Ref. 1, p. 277.
10. Z. S. Basinski: *Proc. Roy. Soc.*, 1957, vol. A240, p. 229.
11. G. Y. Chin, W. F. Hosford, and W. A. Backofen: *Trans. AIME*, 1964, vol. 230, p. 437, p. 1043.
12. A. S. Argon: in *The Inhomogeneity of Plastic Flow*, R. E. Reed-Hill, ed., American Soc. for Metals, Metals Park, OH, 1973, p. 161.
13. M. R. Staker: *Acta Metall.*, 1981, vol. 29, p. 683.
14. T. A. C. Stock and K. R. L. Thompson: *Metall. Trans.*, 1970, vol. 1, p. 219.
15. G. Thomas and R. H. Willens: *Acta Metall.*, 1964, vol. 12, p. 191.
16. J. V. Craig and T. A. C. Stock: *J. Austr. Inst. Met.*, 1970, vol. 15, p. 1.
17. R. C. Glenn and W. C. Leslie: *Metall. Trans.*, 1971, vol. 2, p. 2945.
18. A. L. Wingrove: *J. Austr. Inst. Met.*, 1971, vol. 16, p. 67.
19. Y. Me-Bar and D. Shechtman: *Mat. Sci. Eng.*, 1983, vol. 58, p. 181.
20. A. L. Wingrove: *Metall. Trans.*, 1973, vol. 4, p. 1829.
21. P. S. DeCarli and M. A. Meyers: source cited in Ref. 1, p. 361.
22. M. E. Backman: *Terminal Ballistics*, Naval Weapons Center, China Lake, CA, 1976, p. 74.
23. J. A. Zukas, T. Nicholas, H. F. Swift, L. B. Greszczuk, and D. R. Curran: *Impact Dynamics*, John Wiley, New York, NY, 1982, p. 164.
24. M. A. Meyers and C. T. Aimone: *Prog. in Matls. Sci.*, 1983, vol. 28, no. 1, p. 1.
25. Source cited in Ref. 7, p. 73.
26. R. L. Woodward: *Metal. Trans. A*, 1979, vol. 10A, p. 569.
27. G. L. Moss: source cited in Ref. 1, p. 299.
28. R. E. Winter: *Phil. Mag.*, 1975, vol. 31 (4), p. 765.
29. S. A. Manion and A. L. Wingrove: *J. Austr. Inst. Met.*, 1972, vol. 17, p. 158.
30. M. K. Koul and J. F. Breedis: in *The Science, Technology and Application of Titanium*, R. I. Jaffee and N. E. Promisel, eds., Pergamon Press, New York, NY, 1968, p. 817.
31. M. von Heimendahl: *Electron Microscopy of Metals*, Academic Press, New York, NY, Materials Science Series, A. S. Nowick, ed., translated by U. E. Wolff, 1980, p. 95.